Proceedings of the
47th IEEE Conference on Decision and Control
Cancun, Mexico, Dec. 9-11, 2008

Collective Motion from Consensus with Cartesian Coordinate Coupling - Part I: Single-integrator Kinematics

Wei Ren

Abstract— **This is the first part of a two-part paper on collective motion from consensus with Cartesian coordinate coupling. Collective motions including rendezvous, circular patterns, and logarithmic spiral patterns can be achieved by introducing Cartesian coordinate coupling to existing consensus algorithms. In this first part, we study the collective motions of a team of vehicles in 3D by introducing a rotation matrix to an existing consensus algorithm for single-integrator kinematics. It is shown that both the network topology and the value of the Euler angle affect the resulting collective motions. We show that when the nonsymmetric Laplacian matrix has certain properties and the Euler angle is below, equal, or above a critical value, the vehicles will eventually rendezvous, move on circular orbits, or follow logarithmic spiral curves. In particular, when the vehicles eventually move on circular orbits, the relative radius of the orbits (respectively, the relative phase of the vehicles on their orbits) is equal to the relative magnitude (respectively, the relative phase) of the components of a right eigenvector associated with a critical eigenvalue of the nonsymmetric Laplacian matrix. Simulation results are presented to demonstrate the theoretical results.**

I. Introduction

Coordination of robotic networks has received significant attention in recent years due to its potential impact in numerous civilian, homeland security, and military applications. Examples include space-based interferometry, environment monitoring, border patrol, and search and rescue. Consensus plays an important role in achieving distributed coordination (see [1] and references therein). The basic idea of consensus is that a team of vehicles reaches an agreement on a common value by negotiating with their neighbors.

Related to consensus is the cyclic pursuit strategy, where each vehicle pursues only one other vehicle with the network topology forming a unidirectional ring. Cyclic pursuit is studied for single-integrator kinematics in [2], [3] while for wheeled vehicles subject to nonholonomic constraints in [4], [5]. Ref. [6] generalizes the cyclic pursuit strategy by letting each vehicle pursue one other vehicle along the line of sight rotated by a common offset angle. It is shown that depending on the common offset angle, the vehicles can achieve different symmetric formations, namely, convergence to a single point, a circle, or a logarithmic spiral pattern. Other researchers also study symmetric formations by adopting models based on the Frenet-Serret equations of motion [7] or by exploring the connections between phase models of coupled oscillators and kinematic models of self-propelled particle groups [8].

Motivated by [6], we introduce Cartesian coordinate coupling to existing consensus algorithms. In particular, the Cartesian coordinates of the relative positions of neighboring vehicles are coupled through a rotation matrix in the resulting algorithms. This is the first part of a two-part paper. In this part, we consider the case of single-integrator kinematics while the case of double-integrator dynamics will be dealt with in the second part [9]. In contrast to the existing consensus algorithms for single-integrator kinematics, where the Cartesian coordinates of a vehicle are decoupled, different collective motions can result from the Cartesian coordinate coupling. In contrast to [6], which focuses on a unidirectional ring topology in 2D for single-integrator kinematics, this first part of the paper studies the collection motions resulting from the Cartesian coordinate coupling for single-integrator kinematics over a general network topology in 3D.

The contributions of this first part of the paper are as follows. We study the convergence properties of a consensus algorithm with a rotation matrix introduced in 3D for single-integrator kinematics over a general network topology. We show that both the network topology and the value of the Euler angle affect the resulting collective motions. We show that when the nonsymmetric Laplacian matrix has certain properties and the Euler angle is below, equal, or above a critical value, the vehicles will eventually rendezvous, move on circular orbits, or follow logarithmic spiral curves. In particular, when the vehicles eventually move on circular orbits, the relative radius of the orbits (respectively, the relative phase of the vehicles on their orbits) is equal to the relative magnitude (respectively, the relative phase) of the components of a right eigenvector associated with a critical eigenvalue of the nonsymmetric Laplacian matrix. Our analysis relies on algebraic graph theory, matrix theory, and properties of the Kronecker product. In particular, we will show that the convergence result in [6] is a special case of the result in this part of the paper and the convergence result in [6] can be recovered by exploiting the properties of circulant matrices and the Kronecker product.

II. Background and Preliminaries

A. Graph Theory Notions

It is natural to model interaction among vehicles by directed or undirected graphs. Suppose that a team consists of n vehicles. A weighted graph $\mathcal{G}$ consists of a node set $\mathcal{V} = \{1, \ldots, n\}$, an edge set $\mathcal{E} \subseteq \mathcal{V} \times \mathcal{V}$, and a weighted adjacency matrix $\mathcal{A} = [a_{ij}] \in \mathbb{R}^{n \times n}$. An edge (i, j) in a

W. Ren is with the Department of Electrical and Computer Engineering, Utah State University, Logan, UT 84322, USA wren@engineering.usu.edu

This work was supported by a National Science Foundation CAREER Award (ECCS-0748287).

weighted directed graph denotes that vehicle j can obtain information from vehicle i, but not necessarily vice versa. In contrast, the pairs of nodes in a weighted undirected graph are unordered, where an edge (i,j) denotes that vehicles i and j can obtain information from each another. Weighted adjacency matrix $\mathcal{A}$ of a weighted directed graph is defined such that a_{ij} is a positive weight if $(j,i) \in \mathcal{E}$, while $a_{ij} = 0$ if $(j,i) \notin \mathcal{E}$. Weighted adjacency matrix $\mathcal{A}$ of a weighted undirected graph is defined analogously except that $a_{ij} = a_{ji}$, $\forall i \neq j$, since $(j,i) \in \mathcal{E}$ implies $(i,j) \in \mathcal{E}$.

A directed path is a sequence of edges in a directed graph of the form $(i_1,i_2),(i_2,i_3),\ldots$, where $i_j \in \mathcal{V}$. An undirected path in an undirected graph is defined analogously. A directed graph has a directed spanning tree if there exists at least one node having a directed path to all other nodes. An undirected graph is connected if there is an undirected path between every pair of distinct nodes.

Let nonsymmetric Laplacian matrix [10] $\mathcal{L} = [\ell_{ij}] \in \mathbb{R}^{n\times n}$ associated with $\mathcal{A}$ be defined as $\ell_{ii} = \sum_{j=1,j\neq i}^{n} a_{ij}$ and $\ell_{ij} = -a_{ij}$, $i \neq j$. For a weighted undirected graph, $\mathcal{L}$ is symmetric positive semi-definite. However, $\mathcal{L}$ for a weighted directed graph does not have this property.

B. Existing Consensus Algorithm

Consider vehicles with single-integrator kinematics given by

$$\dot{r}_i = u_i, \quad i = 1,\ldots,n, \tag{1}$$

where $r_i \in \mathbb{R}^m$ is the position and $u_i \in \mathbb{R}^m$ is the control input associated with the ith vehicle. A consensus algorithm for (1) is studied in [11]–[13] as

$$u_i = -\sum_{j=1}^{n} a_{ij}(r_i - r_j), \quad i = 1,\ldots,n, \tag{2}$$

where a_{ij} is the (i,j)th entry of weighted adjacency matrix $\mathcal{A}$ associated with weighted directed graph $\mathcal{G}$. Consensus is reached using (2) if for all $r_i(0)$, $r_i(t) \to r_j(t)$ as $t \to \infty$.

III. Consensus for single-integrator kinematics with Cartesian coordinate coupling

In this section, we consider a consensus algorithm for single-integrator kinematics (1) with Cartesian coordinate coupling as

$$u_i = -\sum_{j=1}^{n} a_{ij}C(r_i - r_j), \quad i = 1,\ldots,n, \tag{3}$$

where $C \in \mathbb{R}^{m\times m}$ denotes a Cartesian coordinate coupling matrix. Note that (2) corresponds to the case where $C = I_m$, where I_m denotes the $m \times m$ identity matrix. That is, using (2), the components of r_i (i.e., the Cartesian coordinates of vehicle i) are decoupled while using (3) the components of r_i are coupled. In this section, we focuses on the case where C is a rotation matrix while a similar analysis can be extended to the case where C is a general matrix.

Using (3), (1) can be written in matrix form as

$$\dot{r} = -(\mathcal{L} \otimes C)r, \tag{4}$$

where $r = [r_1^T,\ldots,r_n^T]^T$, $\mathcal{L}$ is the nonsymmetric Laplacian matrix associated with $\mathcal{G}$, and $\otimes$ denotes the Kronecker product.

Before moving on, we need the following lemmas and definition:

Lemma 3.1: [14] Let $U \in \mathbb{R}^{p\times p}$, $V \in \mathbb{R}^{q\times q}$, $X \in \mathbb{R}^{p\times p}$, and $Y \in \mathbb{R}^{q\times q}$. Then $(U\otimes V)(X\otimes Y) = UX\otimes VY$. Let $A \in \mathbb{R}^{p\times p}$ have eigenvalues β_i with associated eigenvectors $f_i \in \mathbb{C}^p$, $i = 1,\ldots,p$, and let $B \in \mathbb{R}^{q\times q}$ have eigenvalues ρ_j with associated eigenvectors $g_j \in \mathbb{C}^q$, $j = 1,\ldots,q$. Then the pq eigenvalues of $A \otimes B$ are $\beta_i\rho_j$ with associated eigenvectors $f_i \otimes g_j$, $i = 1,\ldots,p$, $j = 1,\ldots,q$.

Lemma 3.2: [13] Let $\mathcal{L}$ be the nonsymmetric Laplacian matrix associated with weighted directed graph $\mathcal{G}$. Then $\mathcal{L}$ has at least one zero eigenvalue and all nonzero eigenvalues have positive real parts. Furthermore, $\mathcal{L}$ has a simple zero eigenvalue and all other eigenvalues have positive real parts if and only if $\mathcal{G}$ has a directed spanning tree. In addition, there exist $\mathbf{1}_n$, where $\mathbf{1}_n$ is the $n \times 1$ column vector of all ones, satisfying $\mathcal{L}\mathbf{1}_n = 0$ and $\mathbf{p} \in \mathbb{R}^n$ satisfying $\mathbf{p} \geq 0$, $\mathbf{p}^T\mathcal{L} = 0$, and $\mathbf{p}^T\mathbf{1} = 1$.[1]

Lemma 3.3: (see e.g., [15]) Given a rotation matrix $R \in \mathbb{R}^{3\times 3}$, let $\mathbf{a} = [a_1,a_2,a_3]^T$ and θ denote, respectively, the Euler axis (i.e., the unit vector in the direction of rotation) and Euler angle (i.e., the rotation angle). The eigenvalues of R are 1, $e^{\iota\theta}$, and $e^{-\iota\theta}$, where ι denotes the imaginary unit, with the associated right eigenvectors given by, respectively, $\varsigma_1 = \mathbf{a}$, $\varsigma_2 = [(a_2^2+a_3^2)\sin^2(\frac{\theta}{2}), -a_1a_2\sin^2(\frac{\theta}{2}) + \iota a_3\sin(\frac{\theta}{2})|\sin(\frac{\theta}{2})|, -a_1a_3\sin^2(\frac{\theta}{2}) - \iota a_2\sin(\frac{\theta}{2})|\sin(\frac{\theta}{2})|]^T$, and $\varsigma_3 = \bar{\varsigma}_2$, where $\bar{\cdot}$ denotes the complex conjugate of a number. The associated left eigenvectors are, respectively, $\varpi_1 = \varsigma_1$, $\varpi_2 = \overline{\varsigma_2}$, and $\varpi_3 = \overline{\varsigma_3}$.

Definition 3.1: Let μ_i, $i = 1,\ldots,n$, be the ith eigenvalue of $-\mathcal{L}$ with associated right eigenvector w_i and left eigenvector ν_i. Also let $\arg(\mu_i) = 0$ for $\mu_i = 0$ and $\arg(\mu_i) \in (\frac{\pi}{2},\frac{3\pi}{2})$ for all $\mu_i \neq 0$, where $\arg(\cdot)$ denotes the phase of a number. Without loss of generality, suppose that μ_i is labeled such that $\arg(\mu_1) \leq \arg(\mu_2) \leq \cdots \leq \arg(\mu_n)$.[2]

Theorem 3.2: Suppose that weighted directed graph $\mathcal{G}$ has a directed spanning tree. Let the control algorithm for (1) be given by (3), where $r_i = [x_i,y_i,z_i]^T$ and C is the 3×3 rotation matrix R defined in Lemma 3.3. Let μ_i, w_i, ν_i, and $\arg(\mu_i)$ be defined in Definition 3.1, $\mathbf{p}$ be defined in Lemma 3.2, and $\mathbf{a} = [a_1,a_2,a_3]^T$, ς_k, and ϖ_k be defined in Lemma 3.3.

1) If $|\theta| < \theta_s^c$, where $\theta_s^c \triangleq \frac{3\pi}{2} - \arg(\mu_n)$, the vehicles will eventually rendezvous at position $(\mathbf{p}^Tx,\mathbf{p}^Ty,\mathbf{p}^Tz)$, where $x = [x_1,\ldots,x_n]^T$, $y = [y_1,\ldots,y_n]^T$, and $z = [z_1,\ldots,z_n]^T$.

2) If $|\theta| = \theta_s^c$ and $\arg(\mu_n)$ is the unique maximum phase of μ_i, all vehicles will eventually move on circular orbits with center $(\mathbf{p}^Tx,\mathbf{p}^Ty,\mathbf{p}^Tz)$ and period $\frac{2\pi}{|\mu_n|}$. The radius of the orbit for vehicle i is given by $2|w_{n(i)}(\frac{\nu_n^T}{\nu_n^Tw_n} \otimes$

[1] That is, $\mathbf{1}_n$ and $\mathbf{p}$ are, respectively, the right and left eigenvectors of $\mathcal{L}$ associated with the zero eigenvalue.

[2] It follows from Lemma 3.2 that $\mu_1 = 0$, $w_1 = \mathbf{1}_n$, and $\nu_1 = \mathbf{p}$.

$\frac{\varpi_2^T}{\varpi_2^T\varsigma_2})r(0)|\sqrt{a_2^2+a_3^2}\sin^2(\frac{\theta}{2})$, where $w_{n(i)}$ is the ith component of w_n. The relative radius of the orbits is equal to the relative magnitude of $w_{n(i)}$. The relative phase of the vehicles on their orbits is equal to the relative phase of $w_{n(i)}$. The circular orbits are on a plane perpendicular to Euler axis $\mathbf{a}$.

3) If $\arg(\mu_n)$ is the unique maximum phase of μ_i and $\theta_s^c < |\theta| < \frac{3\pi}{2} - \arg(\mu_{n-1})$, all vehicles will eventually move along logarithmic spiral curves with center $(\mathbf{p}^T x, \mathbf{p}^T y, \mathbf{p}^T z)$, growing rate $|\mu_n|\cos(\arg(\mu_n)+|\theta|)$, and period $\frac{2\pi}{|\mu_n \sin(\arg(\mu_n)+|\theta|)|}$. The radius of the logarithmic spiral curve for vehicle i is given by $2|w_{n(i)}(\frac{\nu_n^T}{\nu_n^T w_n} \otimes \frac{\varpi_2^T}{\varpi_2^T\varsigma_2})r(0)|e^{[|\mu_n|\cos(\arg(\mu_n)+|\theta|)]t}\sqrt{a_2^2+a_3^2}\sin^2(\frac{\theta}{2})$. The relative radius of the logarithmic spiral curves is equal to the relative magnitude of $w_{n(i)}$. The relative phase of the vehicles on their curves is equal to the relative phase of $w_{n(i)}$. The logarithmic spiral curves are on a plane perpendicular to Euler axis $\mathbf{a}$.

Proof: It follows from Lemmas 3.1 and 3.3 and Definition 3.1 that the eigenvalues of $-(\mathcal{L}\otimes R)$ are μ_i, $\mu_i e^{\iota\theta}$, and $\mu_i e^{-\iota\theta}$ with associated right eigenvectors $w_i\otimes\varsigma_1$, $w_i\otimes\varsigma_2$, and $w_i\otimes\varsigma_3$, respectively, and associated left eigenvectors $\nu_i\otimes\varpi_1$, $\nu_i\otimes\varpi_2$, and $\nu_i\otimes\varpi_3$, respectively. That is, the eigenvalues of $-(\mathcal{L}\otimes R)$ correspond to the eigenvalues of $-\mathcal{L}$ rotated by angles 0, θ, and $-\theta$, respectively. Let λ_ℓ, $\ell=1,\ldots,3n$, denote the ℓth eigenvalue of $-(\mathcal{L}\otimes R)$. Without loss of generality, let $\lambda_{3i-2}=\mu_i$, $\lambda_{3i-1}=\mu_i e^{\iota\theta}$, and $\lambda_{3i}=\mu_i e^{-\iota\theta}$, $i=1,\ldots,n$. Because weighted directed graph $\mathcal{G}$ has a directed spanning tree, it follows from Lemma 3.2 that $-\mathcal{L}$ has a simple zero eigenvalue and all other eigenvalues have negative real parts. According to Definition 3.1, we let $\mu_1=0$ and $\mathrm{Re}(\mu_i)<0$, $i=2,\ldots,n$, where $\mathrm{Re}(\cdot)$ denotes the real part of a number. Note from Lemma 3.2 that $w_1=\mathbf{1}_n$ and $\nu_1=\mathbf{p}$. Because $\mu_1=0$ and $\mu_i\neq 0$, $i=2,\ldots,n$, it follows that $-(\mathcal{L}\otimes R)$ has exactly three zero eigenvalues (i.e., $\lambda_1=\lambda_2=\lambda_3=0$).

Note that $-(\mathcal{L}\otimes R)$ can be written in Jordan canonical form as MJM^{-1}, where the columns of M, denoted by m_k, $k=1,\ldots,3n$, can be chosen to be the right eigenvectors or generalized right eigenvectors of $-(\mathcal{L}\otimes R)$ associated with eigenvalue λ_i, the rows of M^{-1}, denoted by p_k^T, $k=1,\ldots,3n$, can be chosen to be the left eigenvectors or generalized left eigenvectors of $-(\mathcal{L}\otimes R)$ associated with eigenvalue λ_i such that $p_k^T m_k=1$ and $p_k^T m_\ell=0$, $k\neq\ell$, and J is the Jordan block diagonal matrix with λ_i being the diagonal entries. Noting that $\lambda_k=0$, $k=1,2,3$, we can choose $m_k=\mathbf{1}\otimes\varsigma_k$ and $p_k=\mathbf{p}\otimes\frac{\varpi_k}{\varpi_k^T\varsigma_k}$, $k=1,2,3$. Note that $e^{-(\mathcal{L}\otimes R)t}=Me^{Jt}M^{-1}$. Also note that $e^{J_\ell t}\to 0$ when J_ℓ is a Jordan block corresponding to an eigenvalue with a negative real part.

For the first statement of the theorem, note that $\mu_1=0$ and $\mathrm{Re}(\mu_i)<0$, $i=2,\ldots,n$. Also note from Definition 3.1 that $\arg(\mu_{\mathrm{i}})\in[\arg(\mu_2),\arg(\mu_{\mathrm{n}})]\subset(\frac{\pi}{2},\frac{3\pi}{2})$, $i=2,\ldots,n$. Noting that all complex eigenvalues of $-\mathcal{L}$ are in conjugate pairs, it follows that $\arg(\mu_2)=2\pi-\arg(\mu_{\mathrm{n}})$. If $|\theta|<\theta_s^c$, then all $\arg(\mu_{\mathrm{i}})$, $\arg(\mu_{\mathrm{i}}\mathrm{e}^{\iota\theta})$, and $\arg(\mu_{\mathrm{i}}\mathrm{e}^{-\iota\theta})$ are within $(\frac{\pi}{2},\frac{3\pi}{2})$, $i=2,\ldots,n$, which implies that $\mathrm{Re}(\lambda_\ell)<0$, $\ell=4,\ldots,3n$. Noting that $\lambda_k=0$, $k=1,2,3$, it follows that $\lim_{t\to\infty}r(t)=\lim_{t\to\infty}e^{-(\mathcal{L}\otimes R)t}r(0)\to(\sum_{k=1}^3 m_k p_k^T)r(0)=(\mathbf{1}\mathbf{p}^T\otimes I_3)r(0)$. It thus follows that $x_i(t)\to\mathbf{p}^T x(0)$, $y_i(t)\to\mathbf{p}^T y(0)$, and $z_i(t)\to\mathbf{p}^T z(0)$ as $t\to\infty$. That is, all vehicles will eventually rendezvous at $(\mathbf{p}^T x(0),\mathbf{p}^T y(0),\mathbf{p}^T z(0))$.

For the second statement of the theorem, if $\theta=\theta_s^c$ (respectively, $\theta=-\theta_s^c$), then μ_n rotated by an angle θ (respectively, $-\theta$) will locate on the imaginary axis, that is, $\lambda_{3n-1}=\mu_n e^{\iota\theta}=-|\mu_n|\iota$ (respectively, $\lambda_{3n}=\mu_n e^{-\iota\theta}=-|\mu_n|\iota$), while $\mu_2=\overline{\mu_n}$ rotated by an angle $-\theta$ (respectively, θ) will also locate on the imaginary axis, that is, $\lambda_6=\mu_2 e^{-\iota\theta}=|\mu_n|\iota$ (respectively, $\lambda_5=\mu_2 e^{\iota\theta}=|\mu_n|\iota$). Because $\arg(\mu_n)$ is the unique maximum phase of μ_i, λ_{3n-1} (respectively, λ_{3n}) and λ_6 (respectively, λ_5) are the only two nonzero eigenvalues of $-(\mathcal{L}\otimes R)$ on the imaginary axis and all other nonzero eigenvalues have negative real parts. In the following, we focus on $\theta=\theta_s^c$ since the analysis for $\theta=-\theta_s^c$ is similar except that the vehicles will move in reverse directions. Note that $\lambda_k=0$, $k=1,2,3$, and $\mathrm{Re}(\lambda_\ell)<0$ for all $\ell\neq 1,2,3,3n-1,6$. Noting that $\lambda_{3n-1}=-|\mu_n|\iota$ and $\lambda_6=|\mu_n|\iota$, we can choose $m_{3n-1}=w_n\otimes\varsigma_2$, $p_{3n-1}=\frac{\nu_n}{\nu_n^T w_n}\otimes\frac{\varpi_2}{\varpi_2^T\varsigma_2}$, $m_6=\overline{m_{3n-1}}$, and $p_6=\overline{p_{3n-1}}$. It follows that $r(t)=e^{-(\mathcal{L}\otimes R)t}r(0)\to(\sum_{k=1}^3 m_k p_k^T+e^{-\iota|\mu_n|t}m_{3n-1}p_{3n-1}^T+e^{\iota|\mu_n|t}m_6 p_6^T)r(0)$ for large t. Define $c(t)=(e^{-\iota|\mu_n|t}m_{3n-1}p_{3n-1}^T+e^{\iota|\mu_n|t}m_6 p_6^T)r(0)$. Let $c_k(t)$ be the kth component of c, $k=1,\ldots,3n$. It follows that $c_{3(i-1)+\ell}(t)=2\mathrm{Re}(e^{-\iota|\mu_n|t}w_{n(i)}\varsigma_{2(\ell)}p_{3n-1}^T r(0))$, where $i=1,\ldots,n$, $\ell=1,2,3$, and $\varsigma_{2(\ell)}$ denotes the ℓth component of ς_2. After some manipulation, it follows that $c_{3(i-1)+\ell}(t)=2|\varsigma_{2(\ell)}w_{n(i)}p_{3n-1}^T r(0)|\cos(|\mu_n|t-\arg(w_{n(i)}p_{3n-1}^T r(0))-\arg(\varsigma_{2(\ell)}))$, $i=1,\ldots,n$, $\ell=1,2,3$. Therefore, it follows that $x_i(t)\to\mathbf{p}^T x(0)+c_{3i-2}(t)$, $y_i(t)\to\mathbf{p}^T y(0)+c_{3i-1}(t)$, and $z_i(t)\to\mathbf{p}^T z(0)+c_{3i}(t)$ for large t. After some manipulation, it can be verified that $\left\|[c_{3i-2}(t),c_{3i-1}(t),c_{3i}(t)]^T\right\|=2|w_{n(i)}p_{3n-1}^T r(0)|\sqrt{a_2^2+a_3^2}\sin^2(\frac{\theta}{2})$, which is a constant. It thus follows that all vehicles will eventually move on circular orbits with center $(\mathbf{p}^T x(0),\mathbf{p}^T y(0),\mathbf{p}^T z(0))$ and period $\frac{2\pi}{|\mu_n|}$. The radius of the orbit for vehicle i is given by $2|w_{n(i)}p_{3n-1}^T r(0)|\sqrt{a_2^2+a_3^2}\sin^2(\frac{\theta}{2})$. Note that the relative radius of the orbits is equal to the relative magnitude of $w_{n(i)}$. In addition, it is straightforward to see that the relative phase of the vehicles on their orbits is equal to the relative phase of $w_{n(i)}p_{3n-1}^T r(0)$, which is equivalent to the relative phase of $w_{n(i)}$. Note from Lemma 3.3 that Euler axis $\mathbf{a}$ is orthogonal to both $\mathrm{Re}(\varsigma_2)$ and $\mathrm{Im}(\varsigma_2)$, where $\mathrm{Re}(\cdot)$ and $\mathrm{Im}(\cdot)$, representing, respectively, the real and imaginary part of a number, are applied componentwise. It can thus be verified that $\mathbf{a}$ is orthogonal to $[c_{3i-2}(t),c_{3i-1}(t),c_{3i}(t)]^T$, which implies that the circular orbits are on a plane perpendicular to $\mathbf{a}$.

For the third statement of the theorem, if $\arg(\mu_n)$ is the unique maximum phase of μ_i and $\theta_s^c<\theta<\frac{3\pi}{2}-\arg(\mu_{n-1})$ (respectively, $\arg(\mu_{n-1})-\frac{3\pi}{2}<\theta<-\theta_s^c$), then μ_n rotated by an angle θ (respectively, $-\theta$) will have a positive real part,

that is, $\lambda_{3n-1} = \mu_n e^{\iota\theta} = |\mu_n| e^{\iota(\arg(\mu_n)+\theta)}$ (respectively, $\lambda_{3n} = \mu_n e^{-\iota\theta} = |\mu_n| e^{\iota(\arg(\mu_n)-\theta)}$), while $\mu_2 = \overline{\mu_n}$ rotated by an angle $-\theta$ (respectively, θ) will also have a positive real part, that is, $\lambda_6 = \mu_2 e^{-\iota\theta} = |\mu_n| e^{-\iota(\arg(\mu_n)+\theta)}$ (respectively, $\lambda_5 = \mu_2 e^{\iota\theta} = |\mu_n| e^{-\iota(\arg(\mu_n)-\theta)}$). In addition, λ_{3n-1} (respectively, λ_{3n}) and λ_6 (respectively, λ_5) are the only two eigenvalues of $-(\mathcal{L} \otimes R)$ with positive real parts and all other nonzero eigenvalues have negative real parts. In the following, we focus on $\theta_s^c < \theta < \frac{3\pi}{2} - \arg(\mu_{n-1})$ since the analysis for $\arg(\mu_{n-1}) - \frac{3\pi}{2} < \theta < -\theta_s^c$ is similar except that all vehicles will move in reverse directions. Note that $\lambda_k = 0$, $k = 1, 2, 3$, $\mathrm{Re}(\lambda_{3n-1}) > 0$, $\mathrm{Re}(\lambda_6) > 0$, and $\mathrm{Re}(\lambda_k) < 0$ otherwise. Similar to the proof of the second statement, define $c(t) = (e^{|\mu_n| e^{\iota(\arg(\mu_n)+\theta)} t} m_{3n-1} p_{3n-1}^T + e^{|\mu_n| e^{-\iota(\arg(\mu_n)+\theta)} t} m_6 p_6^T) r(0)$. Let $c_k(t)$, $k = 1, \ldots, 3n$, be the kth component of $c(t)$. Also let Let $\varrho_i = |w_{n(i)} p_{3n-1}^T r(0)|$ and $\varphi_i = \arg(w_{n(i)} p_{3n-1}^T r(0))$. It follows that $x_i(t) \to \mathbf{p}^T x(0) + c_{3i-2}(t)$, $y_i(t) \to \mathbf{p}^T y(0) + c_{3i-1}(t)$, and $z_i(t) \to \mathbf{p}^T z(0) + c_{3i}(t)$ for large t, where $c_{3(i-1)+\ell}(t) = 2|\varsigma_{2(\ell)}| \varrho_i e^{[|\mu_n| \cos(\arg(\mu_n)+\theta)]t} \cos([|\mu_n| \sin(\arg(\mu_n) + \theta)]t + \varphi_i + \arg(\varsigma_{2(\ell)}))$, $i = 1, \ldots, n$, $\ell = 1, 2, 3$. Similar to the argument for the second statement, it can be verified that $\left\| [c_{3i-2}(t), c_{3i-1}(t), c_{3i}(t)]^T \right\| = 2\varrho_i e^{[|\mu_n| \cos(\arg(\mu_n)+\theta)]t} \sqrt{a_2^2 + a_3^2 \sin^2(\frac{\theta}{2})}$, which is growing with time. It thus follows that all vehicles will eventually move along logarithmic spiral curves. The statement then follows directly. ■

Corollary 3.3: Suppose that weighted directed graph $\mathcal{G}$ has a directed spanning tree. Let the control algorithm for (1) be given by (3), where $r_i = [x_i, y_i]^T$ and C is the 2×2 rotation matrix given by $R(\theta) = \begin{bmatrix} \cos(\theta) & \sin(\theta) \\ -\sin(\theta) & \cos(\theta) \end{bmatrix}$.

1) If $|\theta| < \theta_s^c$, where $\theta_s^c \triangleq \frac{3\pi}{2} - \arg(\mu_n)$, the vehicles will eventually rendezvous at position $(\mathbf{p}^T x, \mathbf{p}^T y)$, where $x = [x_1, \ldots, x_n]^T$, $y = [y_1, \ldots, y_n]^T$, and $\mathbf{p}$ is defined in Lemma 3.2.

2) If $|\theta| = \theta_s^c$ and $\arg(\mu_n)$ is the unique maximum phase of μ_i, all vehicles will eventually move on circular orbits with center $(\mathbf{p}^T x, \mathbf{p}^T y)$ and period $\frac{2\pi}{|\mu_n|}$. The radius of the orbit for vehicle i is given by $2|w_{n(i)}(\frac{\nu_n^T}{\nu_n^T w_n} \otimes [\frac{1}{2}, -\frac{1}{2}\iota]) r(0)|$. The relative radius of the orbits is equal to the relative magnitude of $w_{n(i)}$. The relative phase of the vehicles on their orbits is equal to the relative phase of $w_{n(i)}$.

3) If $\arg(\mu_n)$ is the unique maximum phase of μ_i and $\theta_s^c < |\theta| < \frac{3\pi}{2} - \arg(\mu_{n-1})$, all vehicles will eventually move along logarithmic spiral curves with center $(\mathbf{p}^T x, \mathbf{p}^T y)$, growing rate $|\mu_n| \cos(\arg(\mu_n) + |\theta|)$, and period $\frac{2\pi}{|\mu_n \sin(\arg(\mu_n)+|\theta|)|}$. The radius of the logarithmic spiral curve for vehicle i is given by $2|w_{n(i)}(\frac{\nu_n^T}{\nu_n^T w_n} \otimes [\frac{1}{2}, -\frac{1}{2}\iota]) r(0)| e^{[|\mu_n| \cos(\arg(\mu_n)+|\theta|)]t}$. The relative radius of the logarithmic spiral curves is equal to the relative magnitude of $w_{n(i)}$. The relative phase of the vehicles on their curves is equal to the relative phase of $w_{n(i)}$.

Proof: The eigenvalues of $R(\theta)$ are given by $e^{\iota\theta}$ and $e^{-\iota\theta}$, with associated right eigenvectors $[1, \iota]^T$ and $[1, -\iota]^T$ and left eigenvectors $[1, -\iota]^T$ and $[1, \iota]^T$, respectively. The rest of the proof follows from that of Theorem 3.2. ■

Corollary 3.4: Suppose that weighted directed graph $\mathcal{G}$ is a unidirectional ring (i.e., a cyclic pursuit topology). Also suppose that $a_{ij} = 1$ if $(j, i) \in \mathcal{E}$ and $a_{ij} = 0$ otherwise. Let the control algorithm for (1) be given by (3), where r_i and C are given as in Corollary 3.3.

1) If $|\theta| < \frac{\pi}{n}$, the vehicles will eventually rendezvous at position $(\mathbf{p}^T x, \mathbf{p}^T y)$, where x and y are given as in Corollary 3.3.

2) If $|\theta| = \frac{\pi}{n}$, all vehicles will eventually move on the same circular orbit with center $(\mathbf{p}^T x, \mathbf{p}^T y)$, period $\frac{\pi}{\sin(\pi/n)}$, and radius $2|w_{n(i)}(\frac{\nu_n^T}{\nu_n^T w_n} \otimes [\frac{1}{2}, -\frac{1}{2}\iota]) r(0)|$.[3] In addition, the vehicles will eventually be evenly distributed on the orbit.

3) If $\frac{\pi}{n} < |\theta| < \frac{2\pi}{n}$, all vehicles will eventually move along logarithmic spiral curves with center $(\mathbf{p}^T x, \mathbf{p}^T y)$, growing rate $2\sin(\frac{\pi}{n}) \sin(|\theta| - \frac{\pi}{n})$, period $\frac{\pi}{\sin(\pi/n) \cos(|\theta| - \pi/n)}$, and radius $2|w_{n(i)}(\frac{\nu_n^T}{\nu_n^T w_n} \otimes [\frac{1}{2}, -\frac{1}{2}\iota]) r(0)| e^{2\sin(\frac{\pi}{n}) \sin(|\theta| - \frac{\pi}{n}) t}$. In addition, the phases of all vehicles will eventually be evenly distributed.

Proof: Note that if weighted directed graph $\mathcal{G}$ is a unidirectional ring and $a_{ij} = 1$ if $(j, i) \in \mathcal{E}$ and $a_{ij} = 0$ otherwise, then $\mathcal{L}$ is a circulant matrix. Also note that a circulant matrix can be diagonalized by a Fourier matrix. The proof then follows Corollary 3.3 directly by use of the properties of the eigenvalues of a circulant matrix and the properties of the Fourier matrix. ■

Remark 3.5: Corollary 3.4 was proved in [6] by use of parametric spectral analysis of some special types of circulant matrices. Here we have shown that Corollary 3.4 is a special case of Corollary 3.3 and the convergence result in [6] can be recovered by exploiting the properties of the circulant matrices and the Kronecker product. Note that when $\mathcal{G}$ is a unidirectional ring (i.e., a cyclic pursuit topology) but different positive weights are chosen for a_{ij} when $(j, i) \in \mathcal{E}$, all vehicles will move on orbits with different radii and their phases will not be evenly distributed.

Example 3.6: To illustrate, consider four vehicles with network topology $\mathcal{G}$ shown by Fig. 1. Let $\mathcal{L}$ associated with $\mathcal{G}$ be given by

$$\begin{bmatrix} 1.5 & 0 & -1.1 & -0.4 \\ -1.2 & 1.2 & 0 & 0 \\ -0.1 & -0.5 & 0.6 & 0 \\ -1 & 0 & 0 & 1 \end{bmatrix}. \tag{5}$$

It can be computed that $\theta_s^c = \frac{3\pi}{2} - \arg(\mu_4) = 1.2975$ rad, where $\mu_4 = -1.6737 - 0.4691\iota$ and $\arg(\mu_4) \in (\pi, \frac{3\pi}{2})$. Let R be the rotation matrix corresponding to Euler axis $\mathbf{a} = \frac{1}{14}[1, 2, 3]^T$ and Euler angle $\theta = \theta_s^c$. Figs. 2, 3, and 4 show, respectively, the eigenvalues of $-\mathcal{L}$ and $-(\mathcal{L} \otimes R)$ when $\theta = \theta_s^c - 0.1$, $\theta = \theta_s^c$, and $\theta = \theta_s^c + 0.1$. Note that the eigenvalues of $-(\mathcal{L} \otimes R)$ correspond to the eigenvalues of $-\mathcal{L}$ rotated by angles 0, θ, and $-\theta$. Note that in Fig. 2, all

[3] In this case, all $w_{n(i)}$, $i = 1, \ldots, n$, have the same magnitude.

nonzero eigenvalues of $-(\mathcal{L}\otimes R)$ are in the open left half plane. In Fig. 3, the eigenvalues of $-(\mathcal{L}\otimes R)$ corresponding to μ_4 rotated by an angle θ and $\mu_2=\overline{\mu_4}$ rotated by an angle $-\theta$ are located on the imaginary axis while all other nonzero eigenvalues are located in the open left half plane. In Fig. 4, the eigenvalues of $-(\mathcal{L}\otimes R)$ corresponding to μ_4 rotated by an angle θ and $\mu_2=\overline{\mu_4}$ rotated by an angle $-\theta$ are located in the open right half plane while all other nonzero eigenvalues are located in the open left half plane.

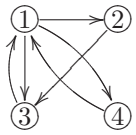

Fig. 1. Network topology for four vehicles. An arrow from j to i denotes that vehicle i can receive information from vehicle j.

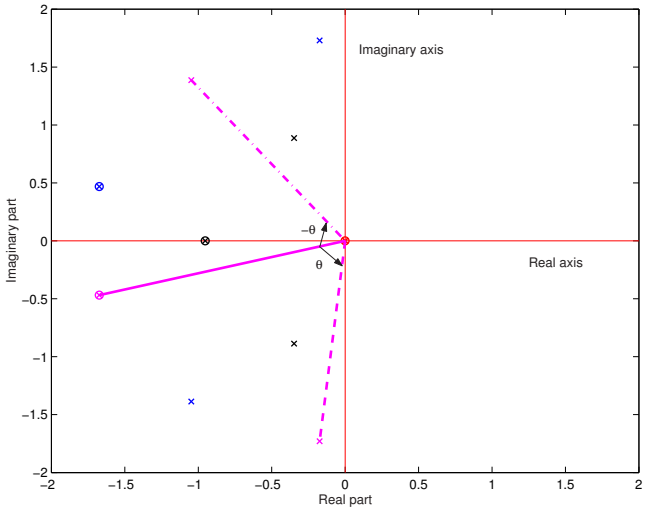

Fig. 2. Eigenvalues of $-\mathcal{L}$ and $-(\mathcal{L}\otimes R)$ with $\theta=\theta_s^c-0.1$. Circles denote the eigenvalues of $-\mathcal{L}$ while x-marks denote the eigenvalues of $-(\mathcal{L}\otimes R)$. The eigenvalues of $-(\mathcal{L}\otimes R)$ correspond to the eigenvalues of $-\mathcal{L}$ rotated by angles 0, θ, and $-\theta$, respectively. In particular, the eigenvalues obtained by rotating μ_4 by angles 0, θ, and $-\theta$ are shown by, respectively, the solid line, the dashed line, and the dashdot line. Because $\theta<\theta_s^c$, all nonzero eigenvalues of $-(\mathcal{L}\otimes R)$ are in the open left half plane.

IV. Simulation

In this section, we study collective motions of four vehicles using (3). Suppose that the network topology is given by Fig. 1 and $\mathcal{L}$ is given by (5). Note that the right eigenvector of $-\mathcal{L}$ associated with eigenvalue μ_4 is $w_4=[-0.2847-0.2820\iota, 0.7213, -0.2501+0.1355\iota, 0.4809+0.0837\iota]^T$. Let θ_s^c and $\mathbf{a}$ be given in Example 3.6.

Figs. 5, 6, and 7 show, respectively, the trajectories of the four vehicles using (3) with $\theta=\frac{\theta_s^c}{2}$, $\theta=\theta_s^c$, and $\theta_s^c+0.1$. Note that the vehicles eventually rendezvous when $\theta=\frac{\theta_s^c}{2}$, move on circular orbits when $\theta=\theta_s^c$, and move along logarithmic spiral curves when $\theta=\theta_s^c+0.1$. Also note that when $\theta=\theta_s^c$, the relative radius of the circular

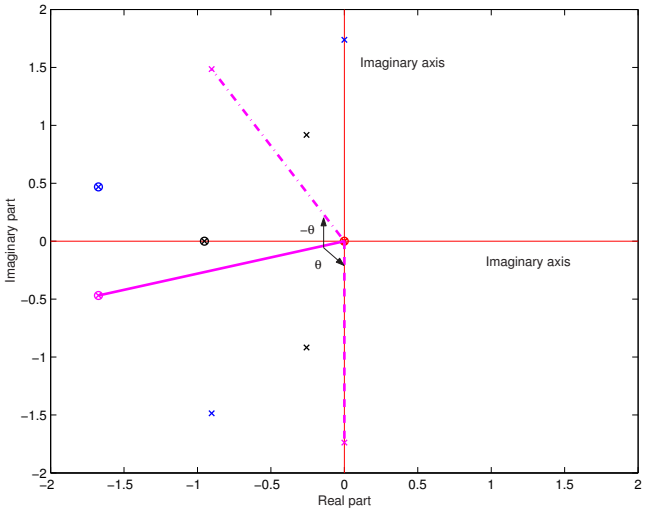

Fig. 3. Eigenvalues of $-\mathcal{L}$ and $-(\mathcal{L}\otimes R)$ with $\theta=\theta_s^c$. Circles denote the eigenvalues of $-\mathcal{L}$ while x-marks denote the eigenvalues of $-(\mathcal{L}\otimes R)$. The eigenvalues of $-(\mathcal{L}\otimes R)$ correspond to the eigenvalues of $-\mathcal{L}$ rotated by angles 0, θ, and $-\theta$, respectively. In particular, the eigenvalues obtained by rotating μ_4 by angles 0, θ, and $-\theta$ are shown by, respectively, the solid line, the dashed line, and the dashdot line. Because $\theta=\theta_s^c$, two nonzero eigenvalues of $-(\mathcal{L}\otimes R)$ are on the imaginary axis.

orbits (respectively, the relative phase of the vehicles) is equal to the relative magnitude (respectively, phase) of the components of w_4. In addition, the trajectories of the vehicles are perpendicular to Euler axis $\mathbf{a}$ in all cases.

V. Conclusion and Future Work

We have introduced Cartesian coordinate coupling to a consensus algorithm by a rotation matrix in 3D for single-integrator kinematics. We have shown conditions under which rendezvous, circular patterns, and logarithmic spiral patterns can be achieved using the algorithm with Cartesian coordinate coupling under a general network topology and quantitatively characterize the resulting collective motions. We have also demonstrated collective motions of four vehicles using the introduced algorithm in simulation. Future work will apply the algorithm in experiments in motion coordination of robotic networks.

References

[1] W. Ren and R. W. Beard, *Distributed Consensus in Multi-vehicle Cooperative Control*, ser. Communications and Control Engineering. London: Springer-Verlag, 2008.

[2] Z. Lin, M. Broucke, and B. Francis, "Local control strategies for groups of mobile autonomous agents," *IEEE Transactions on Automatic Control*, vol. 49, no. 4, pp. 622–629, April 2004.

[3] A. Sinha and D. Ghose, "Generalization of linear cyclic pursuit with application to rendezvous of multiple autonomous agents," *IEEE Transactions on Automatic Control*, vol. 51, no. 11, pp. 1819–1824, November 2006.

[4] J. A. Marshall, M. E. Broucke, and B. A. Francis, "Formations of vehicles in cyclic pursuit," *IEEE Transactions on Automatic Control*, vol. 49, no. 11, pp. 1963–1974, 2004.

[5] ——, "Pursuit formations of unicycles," *Automatica*, vol. 42, no. 1, pp. 3–12, 2006.

[6] M. Pavone and E. Frazzoli, "Decentralized policies for geometric pattern formation and path coverage," *ASME Journal of Dynamic Systems, Measurement, and Control*, vol. 129, no. 5, pp. 633–643, September 2007.

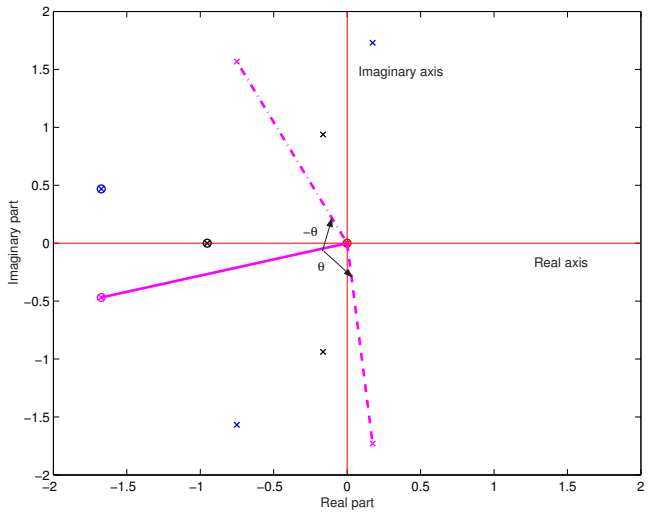

Fig. 4. Eigenvalues of $-\mathcal{L}$ and $-(\mathcal{L}\otimes R)$ with $\theta = \theta_s^c + 0.1$. Circles denote the eigenvalues of $-\mathcal{L}$ while x-marks denote the eigenvalues of $-(\mathcal{L}\otimes R)$. The eigenvalues of $-(\mathcal{L}\otimes R)$ correspond to the eigenvalues of $-\mathcal{L}$ rotated by angles 0, θ, and $-\theta$, respectively. In particular, the eigenvalues obtained by rotating μ_4 by angles 0, θ, and $-\theta$ are shown by, respectively, the solid line, the dashed line, and the dashdot line. Because $\theta > \theta_s^c$, two nonzero eigenvalues of $-(\mathcal{L}\otimes R)$ are in the open right half plane.

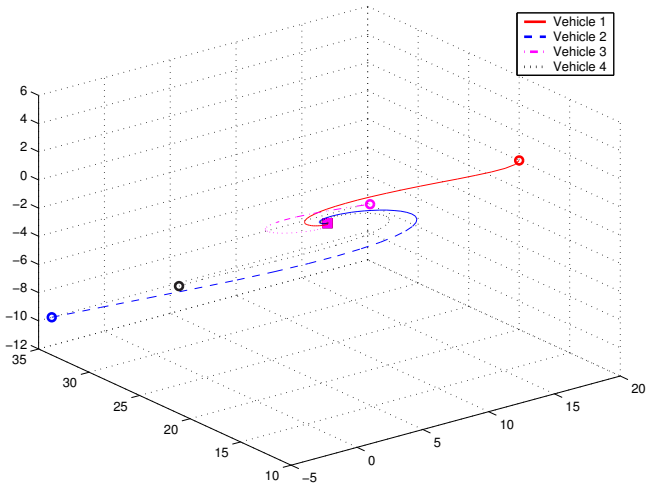

Fig. 5. Trajectories of the four vehicles using (3) with $\theta = \frac{\theta_s^c}{2}$. Circles denote the starting positions of the vehicles while the squares denote the snapshots of the vehicles at 10 sec.

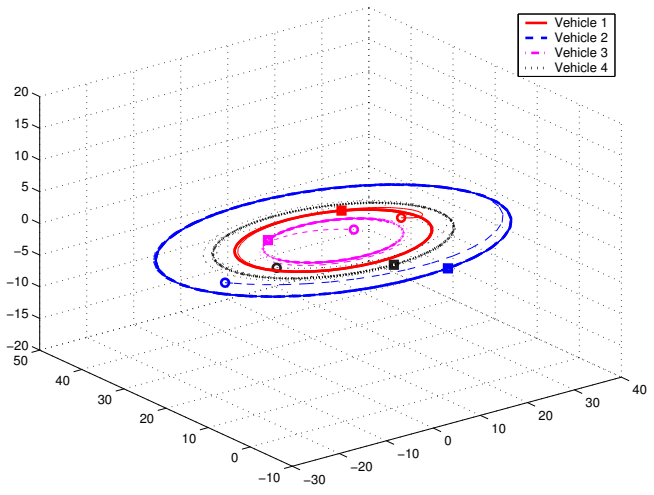

Fig. 6. Trajectories of the four vehicles using (3) with $\theta = \theta_s^c$. Circles denote the starting positions of the vehicles while the squares denote the snapshots of the vehicles at 30 sec.

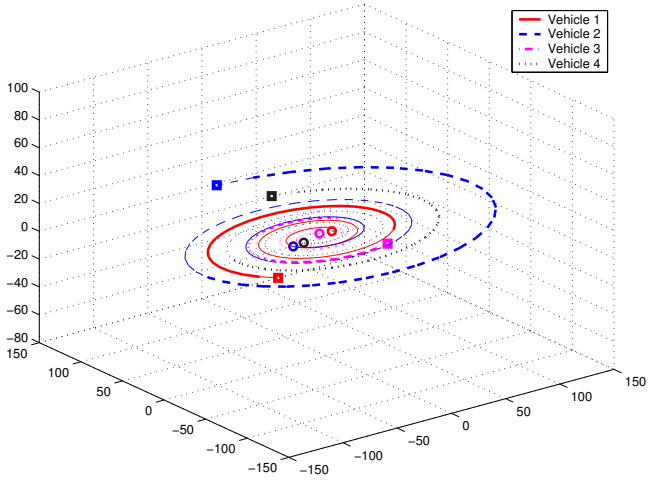

Fig. 7. Trajectories of the four vehicles using (3) with $\theta = \theta_s^c + 0.1$. Circles denote the starting positions of the vehicles while the squares denote the snapshots of the vehicles at 10 sec.

[7] E. W. Justh and P. S. Krishnaprasad, "Equilibria and steering laws for planar formations," *Systems and Control Letters*, vol. 52, pp. 25–38, 2004.
[8] D. A. Paley, N. E. Leonard, R. Sepulchre, D. Grünbaum, and J. K. Parrish, "Oscillator models and collective motion," *IEEE Control Systems Magzine*, vol. 27, no. 4, pp. 89–105, August 2007.
[9] W. Ren, "Collective motion from consensus with Cartesian coordinate coupling - part ii: Double-integrator dynamics," in *Proceedings of the IEEE Conference on Decision and Control*, 2008.
[10] R. Agaev and P. Chebotarev, "On the spectra of nonsymmetric Laplacian matrices," *Linear Algebra and its Applications*, vol. 399, pp. 157–178, 2005.
[11] A. Jadbabaie, J. Lin, and A. S. Morse, "Coordination of groups of mobile autonomous agents using nearest neighbor rules," *IEEE Transactions on Automatic Control*, vol. 48, no. 6, pp. 988–1001, June 2003.
[12] R. Olfati-Saber and R. M. Murray, "Consensus problems in networks of agents with switching topology and time-delays," *IEEE Transactions on Automatic Control*, vol. 49, no. 9, pp. 1520–1533, September 2004.
[13] W. Ren and R. W. Beard, "Consensus seeking in multiagent systems under dynamically changing interaction topologies," *IEEE Transactions on Automatic Control*, vol. 50, no. 5, pp. 655–661, May 2005.
[14] A. J. Laub, *Matrix Analysis for Scientists and Engineers*. Philadelphia, PA: SIAM, 2005.
[15] http://www.mathpages.com/home/kmath593/kmath593.htm.